WMLES of Boundary-Layer Transition

Stephen Woodruff *
NASA Langley Research Center, Hampton, VA 23681

Abstract

The potential for the accurate prediction of laminar-turbulent transition by Wall-Modeled Large-Eddy Simulation (WMLES) is investigated through analysis of Direct Numerical Simulation (DNS) and WMLES results. The analysis indicates satisfactory prediction of transition by WMLES is possible, provided a) a sufficiently accurate wall model for the initial stage of transition is employed, b) a satisfactory transition is made between this initial-stage wall model and the wall model for the downstream fully-developed turbulence, and c) limitations on temporal and spatial resolution, and on the thickness of the wall-modeled region, imposed by the need to accurately resolve the disturbance waves and the transition region are observed. This is illustrated with a WMLES computation that yields reasonable agreement with DNS results; however, the wall-modeled region thickness, and thus the cost savings, is less than is typical for WMLES of fully developed turbulence.

I. Introduction

Wall-modeled large-eddy simulation (WMLES) of the full laminar-turbulent transition process requires that the wall model be effective during the development of the disturbance modes, through the breakdown of discrete disturbances and the development of broader spectrum disturbances and finally the evolution into fully developed turbulence. Wall-resolved large-eddy simulation (WRLES) has been successful,[3] but that success required the use of a dynamic subgrid model. Whether a subgrid model specialized for transitional flows could provide satisfactory results without the cost-intensiveness of a dynamic model, and whether this specialization would be required in the wall-modeled region, in the LES region, or both, remains to be determined. Related work employing DNS to study transition includes the study of H-type, K-type and bypass transition by Wu and Moin,[4] the study of final-stage transition mechanisms in H-type and K-type transitions by Sayadi et al.[5] and the associated reduced-order modeling of Ref. 6, and the work connecting various forms of Parabolized Stability Equation (PSE) analysis, WMLES, WRLES and DNS by Lozano-Duran et al.[12]

In the present paper, analysis of DNS and WMLES results are employed to understand better the requirements for wall and subgrid models employed in WMLES and how they may be met. Spectra and correlations from the DNS results provide insight into the development of the small scales as the transition process unfolds. As these are the scales to be modeled, this information provides evidence as to whether modifications to standard wall and subgrid-scale (SGS) models for fully developed turbulence must be made to the wall model, the SGS model or both, and in what parts of the flow they must be made. Of related interest is the apparent requirement that the dynamic SGS model be employed,[3] suggesting the inertial-range flux behavior during transition is different from that of fully developed turbulence.

WMLES experiments are employed to test the effectiveness of certain transition-modeling concepts to be developed in the following. First, a model for the initial stage of transition is proposed and shown to be effective, provided the wall-modeled region doesn't get too close to the critical layer of the disturbance waves. Second, this initial-stage model is blended with a wall model for fully developed turbulence to yield a full wall model for the transition process. This combined model also yields fairly good results, though the

*Research Scientist, Computational Aerosciences Branch

thickness of the wall-modeled region is smaller than that typically employed in WMLES of fully developed turbulence. The standard (nondynamic) Smagorinsky SGS model is used in these computations.

While the WMLES results presented here are encouraging and represent a significant gain in computational efficiency over DNS or dynamic-model WRLES, the different dynamic characteristics that dominate the early stage of transition, the final stage of transition and fully developed turbulence yield a series of constraints on numerical resolution and models that must be respected in order to perform a successful computation.

II. Problem Description

The H-type subharmonic mode of laminar-turbulent transition has been chosen as the test case for the present investigation. Subharmonic disturbance modes in resonance as a precursor for laminar-turbulent transition were identified by Kachanov and Levchenko[1] in 1984, followed soon by Herbert's stability analysis[2] further clarifying the nature of the modes involved and their interaction. A highly accurate DNS of the disturbance-wave interaction has been presented by Joslin, Streett and Chang.[15]

The subharmonic resonant triad consists of a two-dimensional Tollmein-Schlichting primary wave,

$$u_i = a_{20}\phi_{20,i}(y)E + \text{c.c.}, \tag{1}$$

and two three-dimensional secondary waves,

$$u_i = a_{11}\left(\phi^+_{11,i}(y)e^{i\beta z} + \phi^-_{11,i}(y)e^{-i\beta z}\right)E^{\frac{1}{2}} + \text{c.c.}, \tag{2}$$

where $E = e^{i(\alpha x - \omega t)}$ and α, β and ω are the streamwise and spanwise wavenumbers and the frequency (numerical values are specified below). These waves form a resonant triad: the quadratically nonlinear Navier-Stokes equations generates products of the two secondary waves that force the primary wave and products of the primary wave with each of the secondary waves that force the other secondary wave. This means the effect of the nonlinear interaction is felt at the order of the disturbance amplitude, rather than the disturbance amplitude squared, as would be the case for an arbitrary collection of disturbance waves. The resonant triad interaction is thus capable of initiating transition with much smaller initial disturbance amplitudes.

III. Numerics

The DNS and WMLES computations presented in this paper were performed with a mixed finite-difference/spectral code previously employed in hybrid LES-RANS computations.[7–11] The streamwise and normal directions are discretized on a structured grid with fourth-order finite differences, and the spanwise direction is discretized spectrally. Splitting is employed for time advancement; in the present computations, a Crank-Nicholson/explicit-Runge-Kutta scheme was used for the viscous/convective terms and then the pressure correction is computed from a Poisson equation.

The computational domain is sized following Ref. 12, with inflow boundary at $x = 1$ (where $Re = 180,000$), outflow boundary at $x = 5$, plate surface at $y = 0$ and upper boundary at $y = 0.3535$. All lengths are nondimensionalized by the distance between the plate leading edge and the inflow. The span is the spanwise wavelength of the disturbances introduced at the inflow boundary. For the DNS, the uniform streamwise spacing is $\Delta x^+ = 11.3$ and the number of spanwise modes is 96, corresponding to a uniform grid size of $\Delta z^+ = 5.6$. The first grid point from the wall is at $y^+ = 0.11$. Some of the computations presented below employ only a portion of the full computational domain and the WMLES computations are performed on grids that are coarsened and have near-wall points removed. (Further details will be provided in the discussion below.)

Inflow conditions are specified using the Blasius boundary layer solution and eigenfunction solutions for the disturbances.[13] The frequency and wavenumbers of the disturbances (defined above) are $\omega = 22.311$, $\alpha = 60.695$ and $\beta = 58.447$. The Blasius boundary layer solution is also specified at the upper boundary, following Ref. 12. No-slip conditions are specified at the plate surface and the standard convective boundary condition is used at the outflow boundary.[14]

IV. Direct Numerical Simulation

We begin with some validation computations, involving both the full computational domain and partial-domain computations that will be convenient in the analysis to follow.

IV.A. Initial-Stage DNS

In the initial stage of the computation, the flow is characterized by the Blasius boundary-layer solution perturbed by the relatively small number of plane-wave disturbances that make up the subharmonic resonance triad and their low-order harmonics. These are the waves employed in the successful PSE computations of this stage of transition.[12,13]

DNS for this initial stage of transition employing the code described in the previous section was performed on a truncated section of the computational domain (Figure 1). The region from $x = 1$ to $x = 2.5$ is gridded uniformly as described in the previous section; aggressive grid stretching and a sponge layer following Ref. 15 are employed beyond $x = 2.5$ to reduce reflections from the outflow boundary. Four spanwise modes are employed.

The streamwise evolution of mode amplitudes in Figure 1 shows good agreement with the computations of Ref. 12. The computed mode shapes for the primary and secondary waves at $x = 1.9$ are compared with those computed in Ref. 15 in Figure 2.

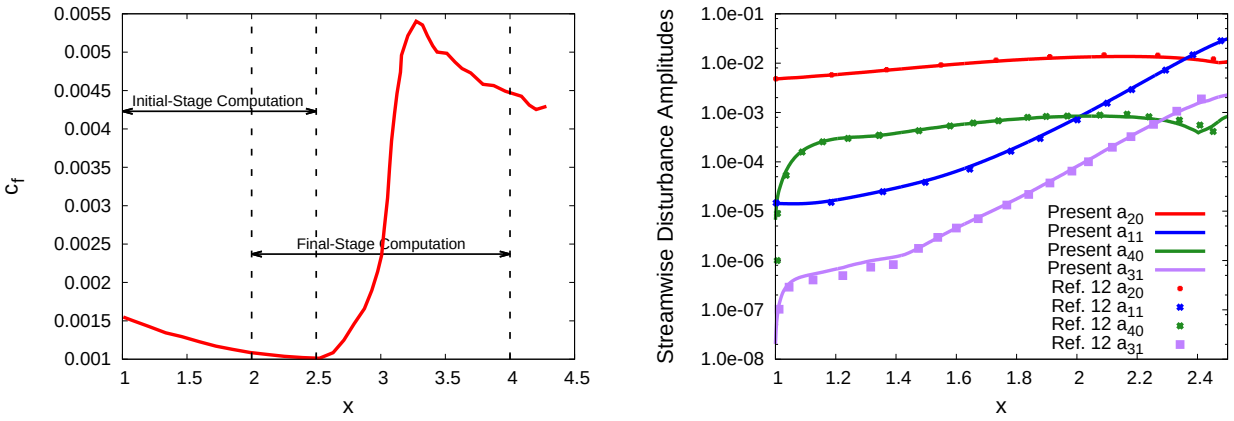


Figure 1. Left: Definition of initial- and final-stage computational domains. Right: Streamwise growth of disturbance-mode amplitudes. Present DNS results compared with those of Ref. 12.

IV.B. Final-Stage DNS

In the final stage of transition, the flow dynamics are characterized by spectrum broadening, an end to small numbers of easily identifiable modes and an evolution into fully developed turbulence. It is convenient for validation purposes, and it will be even more convenient in the WMLES experimentation to follow, to consider this final stage on its own, without computing the full run up to transition in the original computational domain. Thus, the final-stage computations (see Figure 1) will have inflow conditions specified at $x = 2$; these inflow conditions are based on the initial-stage computation discussed above. No grid stretching or sponge layer is employed at the outflow boundary; as the flow is fully turbulent there the convective outflow boundary condition[14] is sufficient. The plots of skin friction and mode amplitudes vs. streamwise position in Figure 3 show the present computation agrees well with that of Ref. 12, once some initial transients are past.

Further comparisons may be made by considering mean-velocity and Reynolds stresses after the flow has reached fully developed turbulence. At the streamwise location $x = 3.8$, for example, the momentum-thickness Reynolds number is about one thousand. The streamwise mean velocity profile there is shown in Figure 4, along with that of the computation of Ref. 12 and that of the DNS of Ref. 16. Reynolds-stress profiles from these computations are shown in Figure 5.

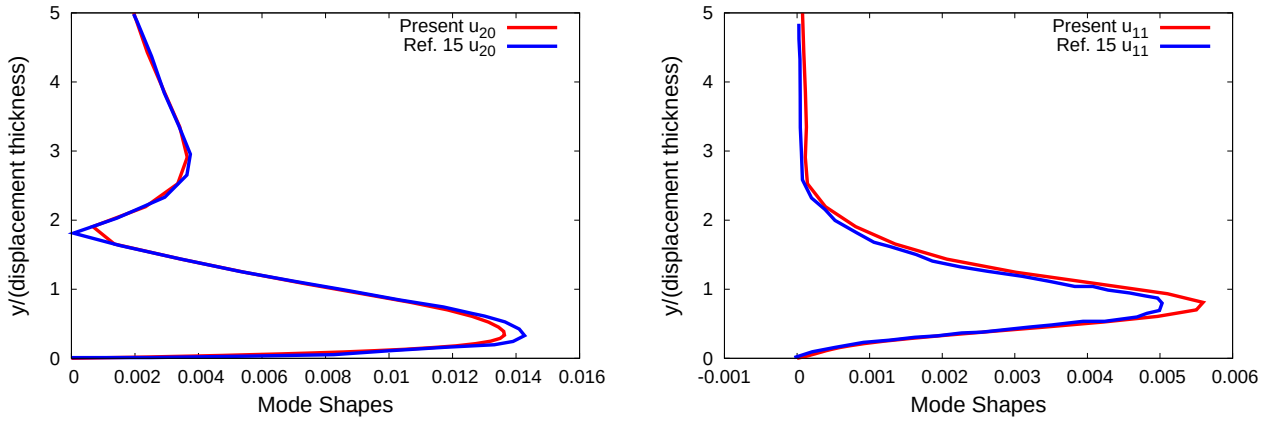


Figure 2. Primary-wave (left) and secondary-wave (right) mode functions (red curves) compared with those of Joslin et al.[15] (blue curves).

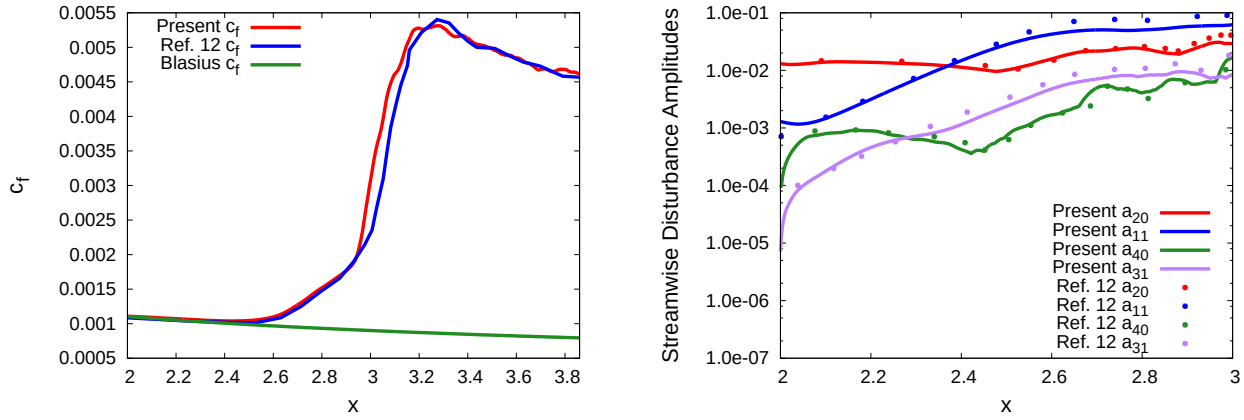


Figure 3. Left: Skin friction from final-stage DNS compared with that of Ref. 12 and Blasius solution. Right: Streamwise evolution of mode amplitudes from final-stage DNS compared with that of Ref. 12.

IV.C. Full-Domain DNS

The final paper will include the results of a full-domain DNS for comparison with the partial-domain computations described above.

IV.D. DNS Analysis

Spectral and correlation data from the full-domain DNS will be analyzed in the final paper, to answer certain questions useful for modeling purposes: Are the smallest scales smaller in final-stage transition than those of the ensuing fully developed turbulence? If so, is this the case in the wall-modeled region, in the LES region, or both? Is there significant anisotropy in these scales? And are there differences in the relation between the dissipation and the inertial-range energy flux, as suggested by the efficacy of the dynamic Smagorinsky model in previous work?

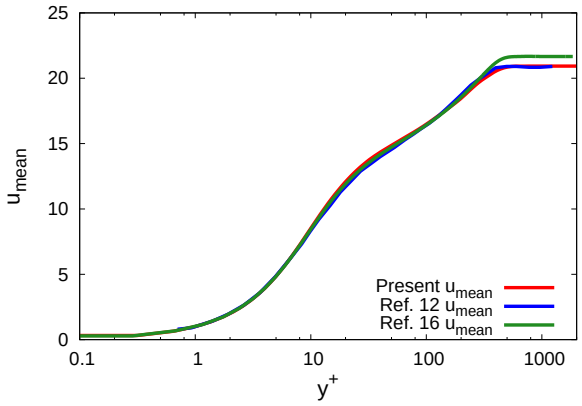


Figure 4. Mean streamwise velocity profile from final-stage DNS at $Re_\theta \approx 1000$ compared with those of Lozano-Duran et al.[12] and Jimenez et al.[16]

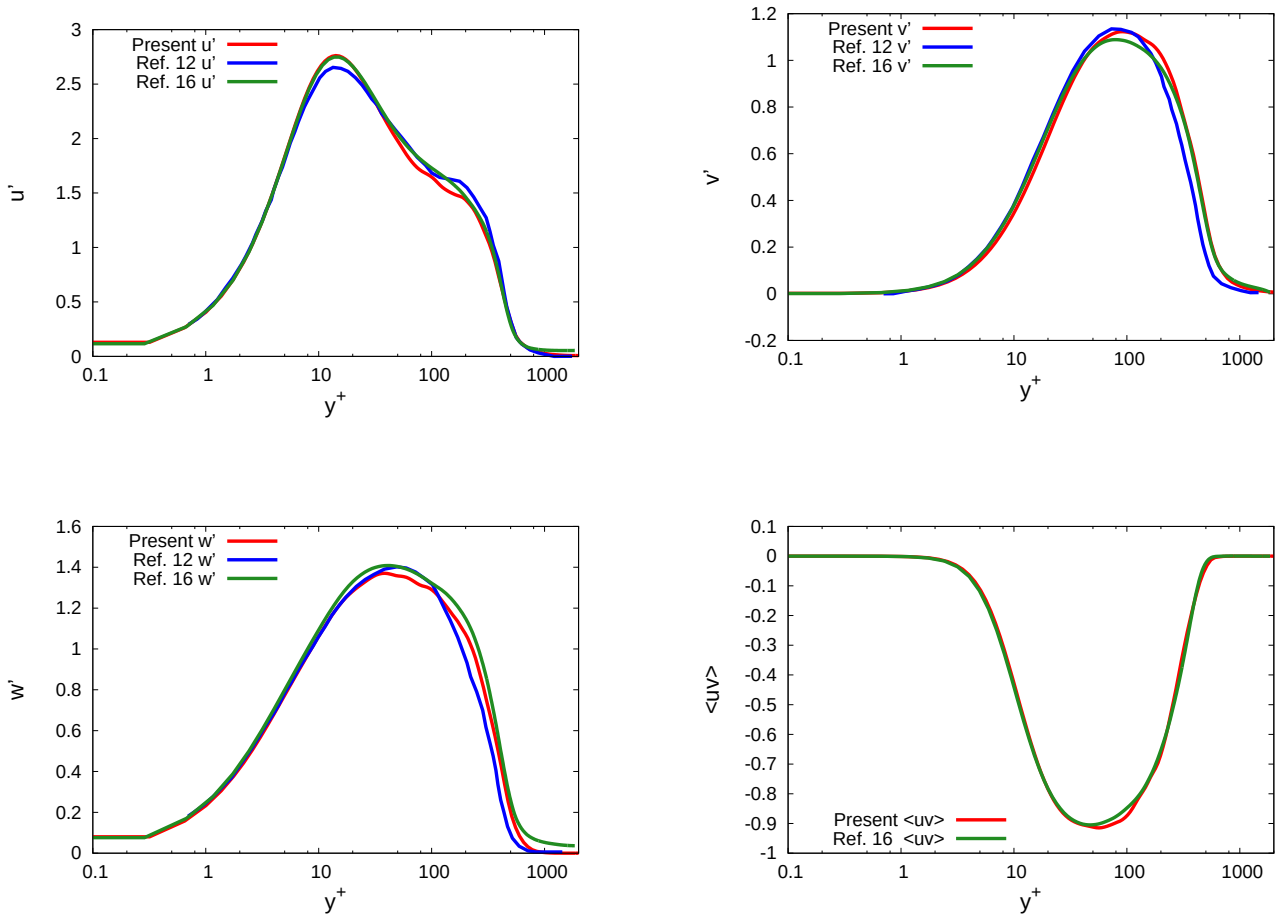


Figure 5. Streamwise (upper left), normal (upper right) and spanwise (lower left) rms velocity profiles and Reynolds shear stress profile (lower right) from final-stage DNS at $Re_\theta \approx 1000$ (red curves) compared with those of Lozano-Duran et al.[12] (blue curves) and Jimenez et al.[16] (green curves).

V. WMLES of Initial-Stage Transition

As introduced by Cabot and Moin,[17] the WMLES wall model is a thin-layer approximation to the Reynolds-averaged Navier-Stokes equations employing a mixing-length model for the eddy viscosity. In

the initial stage of transition, the eddy viscosity is zero and, in the simplest approximation, the thin-layer equations reduce to one-dimensional, parallel-flow, equations for the near-wall flow. This is the analog, in the present context, of the "equilibrium" wall model. While it clearly lacks the physics to capture the dynamics of the critical layer, it provides satisfactory results if the wall-modeled region is entirely below the critical layer (Figure 6). In this computation, the first grid point is at $0.05\delta_0$; the normal spacing is otherwise similar to the DNS grid, as is the streamwise spacing. As in the initial-stage DNS, four spanwise modes are employed.

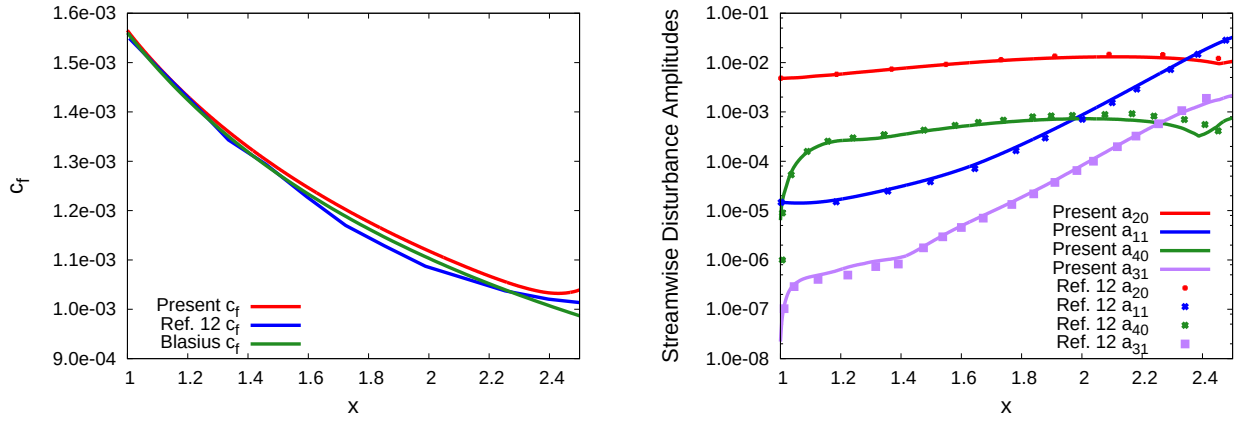


Figure 6. Left: Initial-stage WMLES results for skin friction compared with DNS results of Ref. 12. Right: Streamwise growth of disturbance-mode amplitudes. Initial-stage WMLES results compared with DNS results of Ref. 12.

VI. WMLES of Final-Stage Transition

Applying the same parallel-flow assumptions employed in the previous section to the wall-model equations with an eddy viscosity defined by Prandtl's mixing-length hypothesis (and retaining the molecular viscosity as well) yields a model for the turbulent near-wall region. The ability of this wall model to give reasonable predictions below the log layer is important, because, in keeping with the demonstration of the initial-stage transition wall model in the previous section, the first grid point away from the wall is placed at $0.05\delta_0$, or $y^+ = 5$ at $Re_\theta = 1000$ ($x = 3.8$). This fully developed turbulence wall model is blended with the initial-stage transition wall model as the streamwise skin-friction gradient becomes large. The standard Smagorinsky subgrid-scale model is phased in similarly.

Sixteen spanwise modes are employed in this computation and the time step is twice that of the DNS. The streamwise grid spacing, and the normal distribution of points above the first grid point, follow those of the DNS.

Results from this computation for skin friction and the evolution of the disturbance amplitudes are shown in Figure 7. Agreement with the DNS is good overall, though the rise in c_f is a little early and a little ragged. Mean velocity and Reynolds stress profiles at $Re_\theta = 1000$ are shown in Figures 8 and 9, where agreement is also seen to be good overall, though there is some deterioration in the accuracy of the Reynolds-stress predictions.

It is of interest to note that the fairly good results obtained here are dependent on employing the full turbulence model (both eddy and molecular viscosities) alluded to above, in spite of the fact that the exchange point, $y^+ = 5$, is, at most, at the edge of the viscous sublayer. Use of only the molecular viscosity yields a peak c_f of only about 0.004, suggesting the instantaneous velocity reaches buffer-zone amplitudes sufficiently often to affect the results materially.

Further lengthening of the time step, or increasing the streamwise spacing beyond that of the DNS, appears to noticably degrade the prediction of the primary-wave disturbance amplitude. Thus, even the present relatively modest wall-modeled region thickness has shifted the chief obstacle to an efficient computation from resolution of near-wall flow features to resolution of the primary wave. The flow in the neighborhood of the rise in c_f could well impose similar constraints; the DNS analysis will help clarify this. The final paper

will include additional WMLES computations to quantify the effects of reduced numerical resolution and of increasing the thickness of the wall-model region.

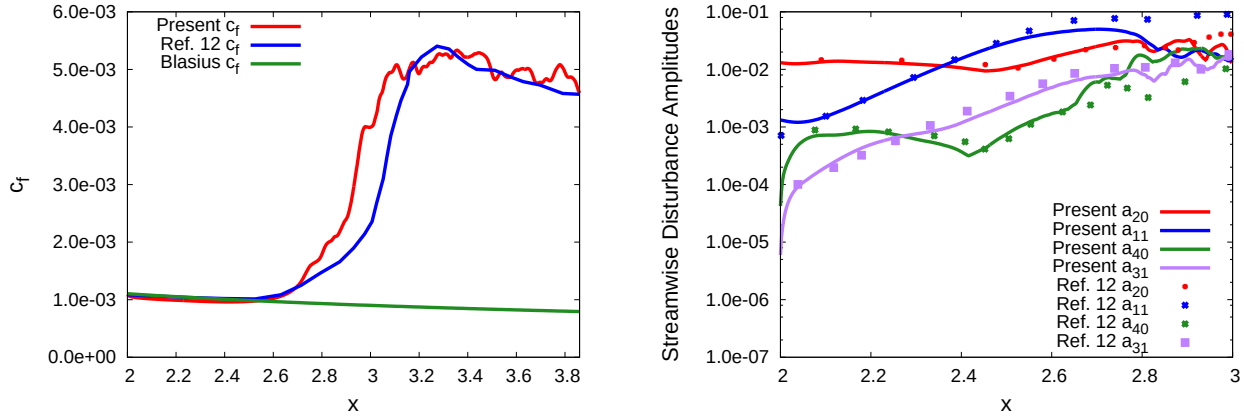


Figure 7. Left: Final-stage WMLES results for skin friction compared with DNS results of Ref. 12. Right: Streamwise growth of disturbance-mode amplitudes. Final-stage WMLES results compared with DNS results of Ref. 12.

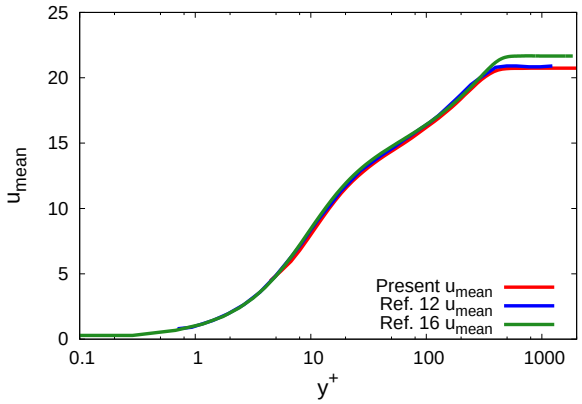


Figure 8. Mean streamwise velocity profile from final-stage WMLES at $Re_\theta \approx 1000$ compared with DNS of Lozano-Duran et al.[12] and Jimenez et al.[16]

VII. Conclusion

As an initial assessment of the potential for WMLES for transition, the results presented here are fairly encouraging. If care is taken to respect the limitations imposed by the different dynamics in the initial and final stages of transition versus the dynamics of fully developed turbulence, significant computational savings are possible. The likely extent of these savings employing the present wall model and the potential for further savings via improved models, will be discussed further in the final paper.

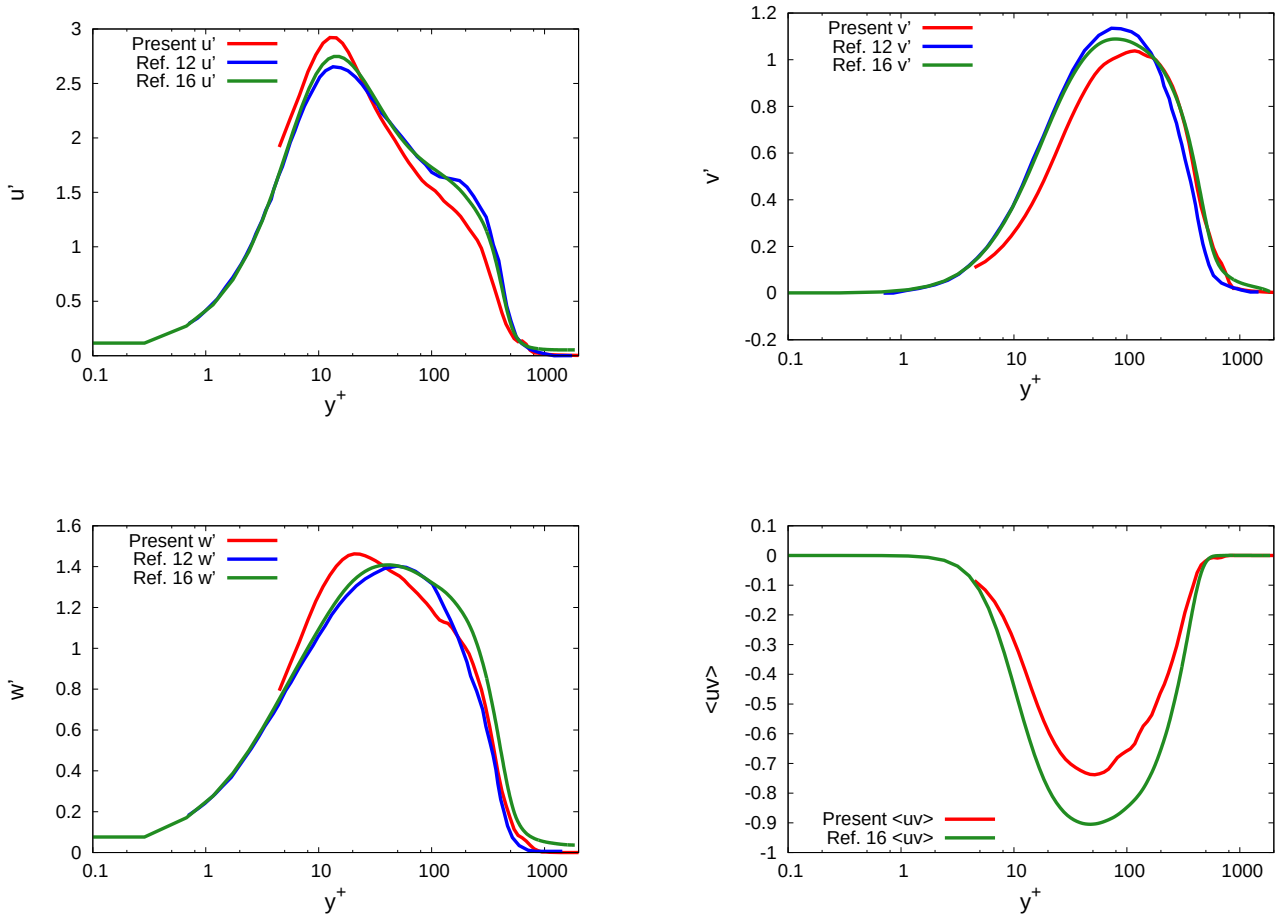


Figure 9. Streamwise (upper left), normal (upper right) and spanwise (lower left) rms velocity profiles and Reynolds shear stress profile (lower right) from final-stage WMLES at $Re_\theta \approx 1000$ (red curves) compared with those of Lozano-Duran et al.[12] (blue curves) and Jimenez et al.[16] (green curves).

References

[1]Kachanov, Yu. S. and Levchenko, V. Ya., "The Resonant Interaction of Disturbances at Laminar-Turbulent Transition in a Boundary Layer," *Journal of Fluid Mechanics* vol. 138, pp. 209–247, 1984.

[2]Herbert, T., "Analysis of the Subharmonic Route to Transition in Boundary Layers," AIAA–84–0009, 1984.

[3]Sayadi, T. and Moin, P., "Large Eddy Simulation of Controlled Transition to Turbulence," *Physics of Fluids* vol. 24, 114103, 2012.

[4]Wu, X. and Moin, P., "Direct Numerical Simulation of Turbulence in a Nominally Zero-Pressure-Gradient Flat-Plate Boundary Layer," *Journal of Fluid Mechanics* vol. 630, pp. 5–41, 2009.

[5]Sayadi, T., Hamman, C. W. and Moin, P., "Direct Numerical Simulation of Complete H-type and K-type Transitions with Implications for the Dynamics of Turbulent Boundary Layers," *Journal of Fluid Mechanics* vol. 724, pp. 480–509, 2013.

[6]Sayadi, T., Schmid, P. J., Nichols, J. W. and Moin, P., "Reduced-Order Representation of Near-Wall Structures in the Late Transitional Boundary Layer," *Journal of Fluid Mechanics* vol. 748, pp. 278–301, 2014.

[7]Woodruff, S. L., "Coupling Turbulence in Hybrid LES-RANS Techniques," *Seventh International Symposium on Turbulence and Shear-Flow Phenomena*, Ottawa, Canada, July 28–31, 2010.

[8]Woodruff, S. L., "A New Formulation for Hybrid LES-RANS Computations," 21st AIAA Computational Fluid Dynamics Conference, June 24-27, 2013, San Diego, CA, AIAA Paper 2013-2722.

[9]Woodruff, S., "Model-Invariant Hybrid LES-RANS Computation of Separated Flow Past Periodic Hills," in *Progress in Hybrid RANS-LES Modelling*, S. Girimaji et al. (eds.), *Notes on Numerical Fluid Mechanics and Multidisciplinary Design*, Vol. 130, Springer, 2015.

[10]Woodruff, S., "Model-Invariant Hybrid Computations of Separated Flows for RCA Standard Test Cases," AIAA SciTech Forum, 54th AIAA Aerospace Sciences Meeting, 4–8 January 2016, San Diego, CA, AIAA 2016–1559.

[11]Woodruff, S., "Adaptive Embedded LES of the NASA Hump," AIAA SciTech 2019 Forum, 7–11 January 2019, San Diego, CA, AIAA 2019–1649.

[12]Lozano-Duran, A., Hack, M. J. P. and Moin, P., "Modeling Boundary-Layer Transition in Direct and Large-Eddy Simulations Using Parabolized Stability Equations," *Physical Review Fluids* vol. 3, 023901 (2018).

[13]Chang, C.–L., "Langley Stability and Analysis Code (LASTRAC) Version 1.2 User Manual," NASA TM–2004–213233, 2004.

[14]Pauley, L. L., Moin, P. and Reynolds, W. C., "The Structure of Two-Dimensional Separation," *Journal of Fluid Mechanics*, vol. 220, 1990, pp. 397–411.

[15]Joslin, R. D., Streett, C. L. and Chang, C.–L., "Spatial Direct Numerical Simulation of Boundary-Layer Transition Mechanisms: Validation of PSE Theory," *Theoretical and Computational Fluid Mechanics* vol. 4, pp 271–288, 1993.

[16]Jimenez, J., Hoyas, S., Simens, M. and Mizuno, Y., "Turbulent Boundary Layers and Channels at Moderate Reynolds Numbers," *Journal of Fluid Mechanics* vol. 657, pp. 335–360, 2010.

[17]Cabot, W. and Moin, P., "Approximate Wall Boundary Conditions in the Large-Eddy Simulation of High Reynolds Number Flow," *Flow, Turbulence and Combustion,* Vol. 63, Nos. 1–4, 2000, pp. 269–291.